

## RESEARCH ARTICLE

10.1002/2016JA023108

## Key Points:

- H-band occurrence peak in the early morning at  $L = 10$ – $12$
- He-band occurrence peak in the afternoon at  $L = 8$ – $10$
- Cold plasma plays a significant role in determining the spectral properties of EMIC waves

## Correspondence to:

K.-H. Kim,  
khan@khu.ac.kr

## Citation:

Kim, G.-J., K.-H. Kim, D.-H. Lee, H.-J. Kwon, and J.-S. Park (2016), Occurrence of EMIC waves and plasmaspheric plasmas derived from THEMIS observations in the outer magnetosphere: Revisit, *J. Geophys. Res. Space Physics*, *121*, 9443–9458, doi:10.1002/2016JA023108.

Received 24 JUN 2016

Accepted 13 SEP 2016

Accepted article online 21 SEP 2016

Published online 8 OCT 2016

## Occurrence of EMIC waves and plasmaspheric plasmas derived from THEMIS observations in the outer magnetosphere: Revisit

Gi-Jeong Kim<sup>1</sup>, Khan-Hyuk Kim<sup>1,2</sup>, Dong-Hun Lee<sup>1</sup>, Hyuck-Jin Kwon<sup>3</sup>, and Jong-Sun Park<sup>4</sup>

<sup>1</sup>School of Space Research, Kyung Hee University, Gyeonggi, South Korea, <sup>2</sup>Research Institute for Sustainable Humanosphere, Kyoto University, Kyoto, Japan, <sup>3</sup>Division of Climate Change Research, Korea Polar Research Institute, Incheon, South Korea, <sup>4</sup>Institute of Space Science, National Central University, Jhongli, Taiwan

**Abstract** We have statistically studied the relationship between electromagnetic ion cyclotron (EMIC) waves and cold plasmaspheric plasma ( $N_{sp}$ ) in the  $L$  range of 6–12 using the Time History of Events and Macroscale Interactions during Substorms (THEMIS) data for 2008–2011. The important observational results are as follows: (1) Under quiet geomagnetic conditions ( $Kp \leq 1$ ), the maximum occurrence rate of the hydrogen (H) band EMIC waves appears in the early morning sector (0600–0900 MLT) at the outermost region ( $L = 10$ – $12$ ). (2) Under moderate and disturbed conditions ( $Kp \geq 2$ ), the H-band occurrence rate is higher in the morning-to-early-afternoon sector for  $L > 10$ . (3) The high-occurrence region of helium (He) band waves for  $Kp \leq 1$  varies from  $L = 7$  to 12 in radial distances along the local time (i.e., at  $L \sim 7$  near noon and at  $L = 8$ – $12$  near late afternoon). (4) The He-band waves for  $Kp \geq 2$  are mainly localized between 1200 and 1800 MLT with a peak around 1500–1600 MLT at  $L = 8$ – $10$ . (5)  $N_{sp}$  is much higher for the He-band intervals than for the H-band intervals by a factor of 10 or more. The He-band high occurrence appears at a steep  $N_{sp}$  gradient region. (6) The morning-afternoon asymmetry of the normalized frequency seen both in H-band and He-band is similar to the asymmetric distribution of  $N_{sp}$  along the local time. These observations indicate that the cold plasma density plays a significant role in determining the spectral properties of EMIC waves. We discuss whether a morning-afternoon asymmetry of the EMIC wave properties can be explained by the spatial distribution of cold plasmaspheric plasma.

### 1. Introduction

Early theoretical works described how proton cyclotron waves with frequencies below the proton gyrofrequency can be generated as transverse left-handed polarized waves in the equatorial region of the magnetosphere by an anisotropic distribution of energetic ( $\sim 10$ – $100$  keV) ring current ions [e.g., Cornwall, 1965; Kennel and Petschek, 1966]. It has been generally accepted that the proton temperature anisotropy is a necessary condition to generate waves. However, recent observations provide that the anisotropy is not the only important factor for the generation of proton cyclotron waves [e.g., Lin et al., 2014].

Since these waves are excited over the Pc1–Pc2 frequency range (0.1–5.0 Hz), it has long been recognized that Pc1–Pc2 geomagnetic pulsations observed on the ground are generated in the magnetosphere by wave-particle interactions [e.g., Bossen et al., 1976; Fraser et al., 1989; Yahnina et al., 2000; Sakaguchi et al., 2008; Kim et al., 2016b]. Spacecraft observations have shown that Pc1–Pc2 waves in the magnetosphere are mostly transverse and left-handed polarized [Anderson et al., 1992a, 1992b; Fraser and Nguyen, 2001; Min et al., 2012], which is the polarization state of the waves expected from the theoretical studies. In the presence of heavy ions ( $\text{He}^+$  and  $\text{O}^+$ ), the waves can be generated in three distinct bands: a H-band between the local  $\text{H}^+$  gyrofrequency ( $f_{\text{H}^+}$ ) and  $\text{He}^+$  gyrofrequency ( $f_{\text{He}^+}$ ), a He-band between the local  $\text{He}^+$  gyrofrequency ( $f_{\text{He}^+}$ ) and  $\text{O}^+$  gyrofrequency ( $f_{\text{O}^+}$ ), and an O-band below  $f_{\text{O}^+}$ . These waves are now identified as electromagnetic ion cyclotron (EMIC) waves.

There have been studies reporting that the cold plasmaspheric density including heavy ions plays an important role in controlling the generation and propagation of EMIC waves because the cold background plasma strongly influences the convective growth rate [e.g., Young et al., 1981; Kozyra et al., 1984; Horne and Thorne, 1994; Chen et al., 2009]. Since an enhanced convective growth rate is expected in a region of dense and cold

plasmaspheric plasma [e.g., Cornwall, 1965; Kennel and Petschek, 1966; Kozyra et al., 1984], the plasmopause has been considered as a preferred region for EMIC wave generation. However, CRRES observations showed that the plasmopause itself is not necessarily the preferred region for wave generation and that the occurrence rate of EMIC waves peaks near the apogee of the spacecraft ( $L = 6-7$ ), which is more outward than a typical plasmopause location ( $L = 4-5$ ), in the afternoon sector [Fraser and Nguyen, 2001]. More extensive statistical studies using Active Magnetospheric Particle Tracer Explorers/Charge Composition Explorer (AMPTE/CCE) data [Anderson et al., 1992a] and Time History of Events and Macroscale Interactions during Substorms (THEMIS) data [Usanova et al., 2012] showed that the highest occurrence rate of EMIC waves appears in the afternoon near the spacecraft apogees ( $L \sim 9$  for AMPTE/CCE and  $L \sim 12$  for THEMIS), which is  $\sim 2-5 R_E$  farther out than the CRRES apogee.

Most recently, statistical studies of inner magnetosphere ( $L < 6$ ) EMIC waves using Van Allen Probes [Saikin et al., 2015, 2016; Wang et al., 2015] and CRRES [Halford et al., 2016] showed that the occurrence rate of EMIC waves increases with radial distance. In the dayside sector between  $L = 4$  and  $L = 6$ , EMIC waves were more frequently detected on Van Allen Probes and CRRES than on AMPTE/CCE and THEMIS by a factor of 2 or more, implying the important role of the plasmopause or plasmaspheric plume in generating EMIC waves. This difference may be due to a by-product of the apogee of the spacecraft.

Magnetospheric compression leads to an increase in temperature anisotropy of energetic ions [e.g., Anderson and Hamilton, 1993], and its effect increases with increasing radial distance, with the maximum just inside the magnetopause. It has been proposed that the radial dependence of EMIC wave occurrence is attributed to solar wind dynamic pressure variations. That is, enhanced solar wind dynamic pressure is one of the main parameters driving EMIC waves during disturbed and quiet times in the outer magnetosphere [e.g., Olson and Lee, 1983; Anderson and Hamilton, 1993; Arnoldy et al., 2005; Engebretson et al., 2002; Usanova et al., 2008; Hyun et al., 2014; Park et al., 2016]. Recent statistical studies of EMIC waves using Cluster data covering all dipole latitudes have reported the existence of off-equator source regions at high  $L$  shell values in the dayside outer magnetosphere for EMIC waves [Allen et al., 2015, 2016]. The authors suggest that such off-equator source regions are due to the compression of the dayside magnetosphere leading the bulk plasma population to execute Shabansky orbits, which play a role in providing the source anisotropy of waves at higher latitudes on the dayside [McCollough et al., 2012].

There are many observations showing the occurrence peak of EMIC waves in the afternoon at a wide  $L$  range from the inner magnetosphere to the outer magnetosphere [Anderson et al., 1992a; Kasahara et al., 1992; Fraser and Nguyen, 2001; Meredith et al., 2003; Clausen et al., 2011; Min et al., 2012; Usanova et al., 2012; Keika et al., 2013; Allen et al., 2015; Saikin et al., 2015, 2016; Park et al., 2016]. It has been suggested that the occurrence rate bias toward the afternoon is probably associated with plasmaspheric plumes [e.g., Chen et al., 2009]. Darrouzet et al. [2008] found that plasmaspheric plumes have a high chance of being detected in the afternoon (MLT = 1500–1600) between  $L = 6$  and  $L = 9$ . The morning-afternoon asymmetry of plume detection rate is qualitatively similar to that of EMIC wave occurrence.

Recently, Posch et al. [2010] and Usanova et al. [2013] reported that EMIC wave occurrence has a weak causal relationship with the plume occurrence. That is, the high-occurrence region of EMIC waves is not consistent with that of plumes. Consequently, the authors concluded that plumes were not necessary for EMIC wave generation. In their studies, however, the occurrence rate of EMIC waves were examined without separating frequency bands (i.e., the H-band and He-band). As pointed out by Kozyra et al. [1984] and Horne and Thorne [1994], cold plasmaspheric plasma plays a significant role in determining the spectral properties of EMIC waves, and the presence of cold  $\text{He}^+$  ions greatly suppresses the H-band wave growth. If H-band waves are suppressed and He-band waves are enhanced by cold plasmas including heavy ions in plumes, then the correspondence between He-band waves and plumes will be high. Thus, a statistical study for the relationship between EMIC waves and plasmaspheric plumes should be done separately for the H-band and He-band.

Keika et al. [2013] reported global distributions of H-band and He-band waves using AMPTE/CCE data over a  $\sim 4.5$  year period. The peak occurrence rate of H-band waves is seen in the early afternoon near the apogee ( $L \sim 9$ ), and the He-band peak rate occurs in the late afternoon sector for  $L = \sim 7-9$ . Global distributions of H-band and He-band waves derived from THEMIS observations are significantly different from those of the AMPTE/CCE observations [Min et al., 2012]. The occurrence rate of H-band waves is clearly peaked in the dawnside sector at  $L = 10-12$  while the He-band peak is seen in the late afternoon near dawn at a wider range of  $L = 8-12$ . This dawn-dusk asymmetry of H-band and He-band EMIC wave occurrences may be due

to the cold plasma distribution in the outer magnetosphere as suggested by *Min et al.* [2012]. Thus, precise knowledge of the cold plasma distribution is critical to understand the properties of EMIC waves.

The objective of the present study is to investigate the relationship between EMIC wave occurrence and the spatial distribution of plasmaspheric plasmas. We note that *Min et al.* [2012] used the plasmaspheric plasma density to examine spatial variations of EMIC wave properties. However, they did not compare plasmaspheric plasma densities associated with EMIC waves separated in the H-band and He-band and thus could not determine how plasmaspheric plasma influences EMIC wave occurrence and their spectral properties. In our study, we compare the plasma densities detected during the H-band and He-band wave intervals, respectively, and discuss how and where the cold plasmaspheric plasma contributes to the wave occurrence and wave spectral properties. Our data analysis was motivated in part by geosynchronous observations, which indicate that the local time occurrence distribution of He-band waves depends on geomagnetic activity [*Park et al.*, 2016]. In this study, we investigate the spatial occurrence distributions for H-band and He-band waves under three different geomagnetic conditions (all  $Kp$ ,  $Kp \geq 2$ , and  $Kp \leq 1$ ). Since O-band EMIC waves in the outer magnetosphere overlap with dayside ultralow frequency pulsations in the Pc3 frequency band ( $\sim 20$ – $100$  mHz), we exclude O-band EMIC waves in this study.

The organization of this paper is as follows. In section 2, we describe the data for this study. In section 3, we examine examples of EMIC waves observed in the outer magnetosphere and describe the event selection procedure. In section 4, we present statistical analyses. In section 5, we discuss the statistical results. Our conclusions are presented in section 6.

## 2. Data Set

The THEMIS probes were launched in February 2007. They were on a low-inclination ( $< 10^\circ$ ) orbit with apogees above  $10 R_E$  and perigees below  $2 R_E$  [*Sibeck and Angelopoulos*, 2008]. This satellite inclination limits the magnetic latitude between  $-20^\circ$  and  $20^\circ$ . Each THEMIS probe carried a triaxial fluxgate magnetometer [*Auster et al.*, 2008]. In this study, we used the magnetic field data of low-resolution mode at four samples per second (0.25 s) measured by THEMIS A, THEMIS D, and THEMIS E in the outer magnetosphere ( $L > 6$ ) over a 4 year period from 2008 to 2011. The THEMIS magnetic field data are displayed in a mean-field-aligned (MFA) coordinate system, where  $\hat{e}_z$  points along the magnetic field, defined to be the low-pass-filtered magnetic field measured using 300 s moving average,  $\hat{e}_y$  (eastward) is parallel to  $\hat{e}_z \times \mathbf{r}$ , where  $\mathbf{r}$  is the spacecraft position vector relative to the center of the Earth, and  $\hat{e}_x$  (radial) is given by  $\hat{e}_x = \hat{e}_y \times \hat{e}_z$ . We used the total electron density inferred from the spacecraft potential and electron thermal speed measured by the Electric Field Instrument [*Bonnell et al.*, 2008] and electrostatic analyzer (ESA) instrument [*McFadden et al.*, 2008] on board THEMIS A, D, and E probes to examine whether the properties of EMIC waves depend on the cold plasma density.

## 3. Example of EMIC Waves and Event Selection

Figures 1a and 1b show the interplanetary magnetic field (IMF)  $B_z$  in geocentric solar magnetospheric (GSM) coordinates and solar wind dynamic pressure ( $P_{sw}$ ), respectively, shifted to the bow shock nose from the Wind spacecraft for 13:00–19:00 UT on 11 August 2009. The IMF  $B_z$  exhibited southward and northward fluctuations between  $+2$  and  $-2$  nT for 13:00–15:15 UT, rotated from north to south at  $\sim 15:15$  UT, and then stayed southward mostly near  $-3$  nT until 19:00 UT.  $P_{sw}$  gradually increased from  $\sim 1.1$  to  $\sim 1.4$  nPa for 13:00–15:00 UT, and was near  $\sim 1.3$  nPa before a sudden increase with a peak of  $\sim 1.7$  nPa at 18:30 UT.

During the 6 h interval, THEMIS D was near the magnetic equator between  $1.4^\circ$  and  $6.3^\circ$  in magnetic latitude (MLAT) and moved outward from  $L = 6.2$  to  $L = 11.1$  in the dayside sector of 11.8–14.3 magnetic local time (MLT). Figure 1c shows the magnetic field intensity observed by THEMIS D and the T05 model field intensity [*Tsyganenko and Sitnov*, 2005] estimated using solar wind conditions at 16:00 UT. There were sudden changes in the observed magnetic field intensity after 18:30 UT, corresponding to the interval of sudden increase in  $P_{sw}$ . These field signatures indicate that THEMIS D transiently entered the magnetosheath. The magnetic field magnitude ( $\Delta B$ ), subtracting the model from the observation, is plotted in Figure 1d. Except for the interval of  $\sim 15:00$ – $16:30$  UT, the observed field intensity was slightly smaller than the model intensity ( $|\Delta B| < \sim 6$  nT).  $\Delta B$  gradually decreased from 13:00 to 14:00 UT and then increased from 14:00 UT to 15:00 UT to a magnitude of  $\sim 5$  nT. This magnetic field distortion is due to the magnetic field compression caused by the increase in  $P_{sw}$ .

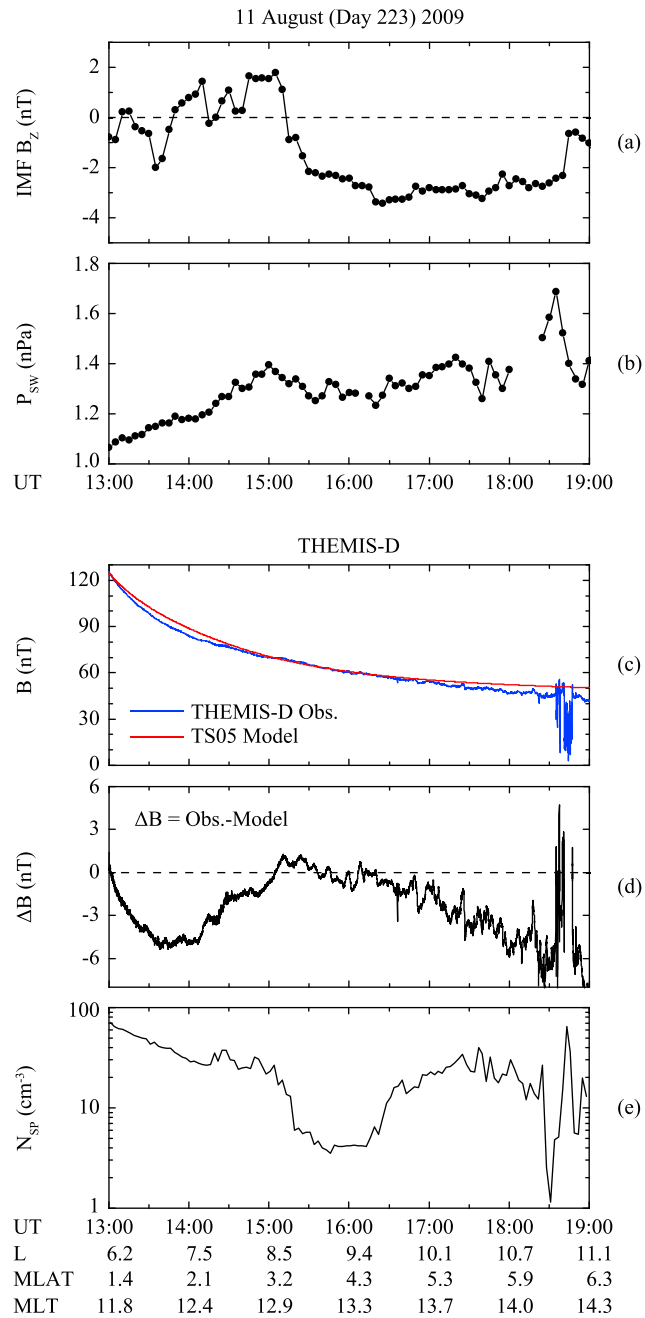


**Figure 1.** Comparison of solar wind parameters at Wind and magnetospheric magnetic field and electron density ( $N_{sp}$ ), inferred from the spacecraft potential, at THEMIS D for the interval from 13:00 to 19:00 UT on 11 August 2009. (a) Interplanetary magnetic field (IMF)  $B_z$  in GSM coordinates. (b) Solar wind dynamic pressure ( $P_{sw}$ ). (c) The magnetic field intensity observed by THEMIS D (blue) and the T05 model field intensity (red). (d) The magnetic field magnitude ( $\Delta B$ ), subtracting the model from the observation. (e) Electron density.

Figure 1e shows the radial profile of electron density ( $N_{sp}$ ), inferred from the THEMIS D spacecraft potential, for the outbound leg. Since  $N_{sp}$  is plasmaspheric (i.e., cold plasma),  $N_{sp}$  has been used to examine the spatial distribution of plasmaspheric plasmas [e.g., Li *et al.*, 2010; Nishimura *et al.*, 2013; Walsh *et al.*, 2013; Kwon *et al.*, 2015].  $N_{sp}$  has a simple radial structure, decreasing as a function of  $L$ , with a slight enhancement around 14:16 UT and a sudden decrease from  $\sim 27 \text{ cm}^{-3}$  at 15:04 UT ( $L = 8.6$ ) to  $\sim 6 \text{ cm}^{-3}$  at 15:19 UT ( $L = 8.8$ ). The plasmapause is usually defined to be a density gradient of a factor of 5 or greater over an  $L$  distance smaller than 0.5 [e.g., Carpenter and Anderson, 1992; Moldwin *et al.*, 2002]. Thus, the sudden decrease in  $N_{sp}$  at  $L = 8.6$  indicates that

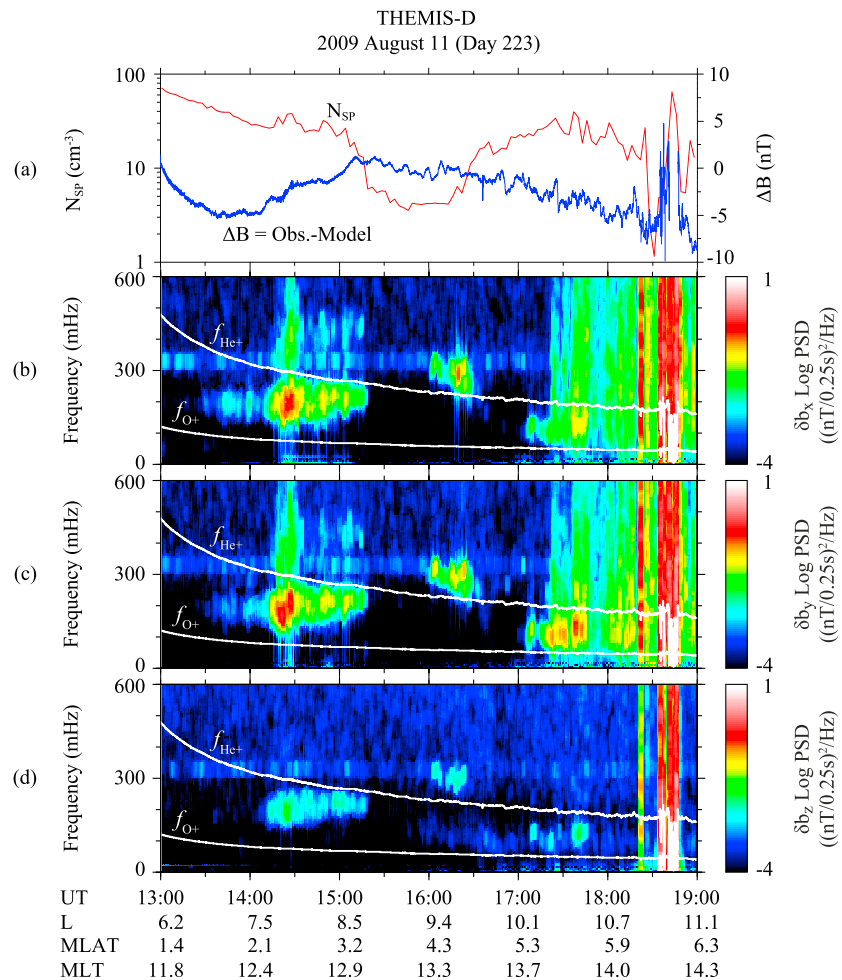


**Figure 2.** (a) Electron density and  $\Delta B$  shown in Figure 1. Dynamic power spectrograms for the THEMIS D magnetic field data for the interval displayed in Figure 1. The three components (b)  $\delta b_x$ , (c)  $\delta b_y$ , and (d)  $\delta b_z$  denote perturbations in the radial, azimuthal, and field-aligned directions, respectively. The data were time differenced prior to spectral estimate in order to remove a slowly varying background. The two white lines in the dynamic spectrograms indicate the local helium ( $f_{He^+}$ ) and oxygen ( $f_{O^+}$ ) gyrofrequencies.

THEMIS D moved across the plasmapause. Since  $Kp$  stayed at low levels between 0+ and 1 for 21 h from 00:00 to 21:00 UT on 11 August 2009, the location of the plasmapause formed at  $L = 8.6$  is not unreasonable [Kwon *et al.*, 2015]. After exiting the plasmasphere, THEMIS D was in a low-density plasma and then reentered the dense plasmaspheric plasma region around 16:30 UT as it was approaching the magnetopause. The dense plasma was observed until just before the transient magnetopause crossing, indicating that the cold plasmaspheric plasma was attached at the magnetopause. Although we cannot determine whether the cold and dense plasmaspheric plasma near the magnetopause is detached from the plasmasphere or connected to the plasmasphere (i.e., plasmaspheric plume), it may be associated with the magnetospheric convection electric field, enhanced during the steady southward IMF interval from 15:30 to 19:00 UT under quiet geomagnetic conditions ( $Kp \leq 1$ ).

Figure 2 shows  $N_{sp}$ ,  $\Delta B$ , and dynamic Fourier spectrograms of the three components (transverse components, radial ( $\delta b_x$ ) and azimuthal ( $\delta b_y$ ), and the compressional ( $\delta b_z$ ) component) of the differenced magnetic field in the MFA coordinates for the interval displayed in Figure 1. The two white lines in dynamic spectrograms represent the local helium ( $f_{He^+}$ ) and oxygen ( $f_{O^+}$ ) gyrofrequencies. The spectra were calculated using a data window of 3 min (720 data points), stepping it forward by 25% (45 s), and smoothed by eight-point averaging. All three components have a frequency band near 330 mHz, which is related to the spin period ( $\sim 3$  s) of the spacecraft. The strongly enhanced spectral intensities in the frequency band from 0 to 600 mHz occurred when the spacecraft briefly entered the magnetosheath and/or boundary layer regions.

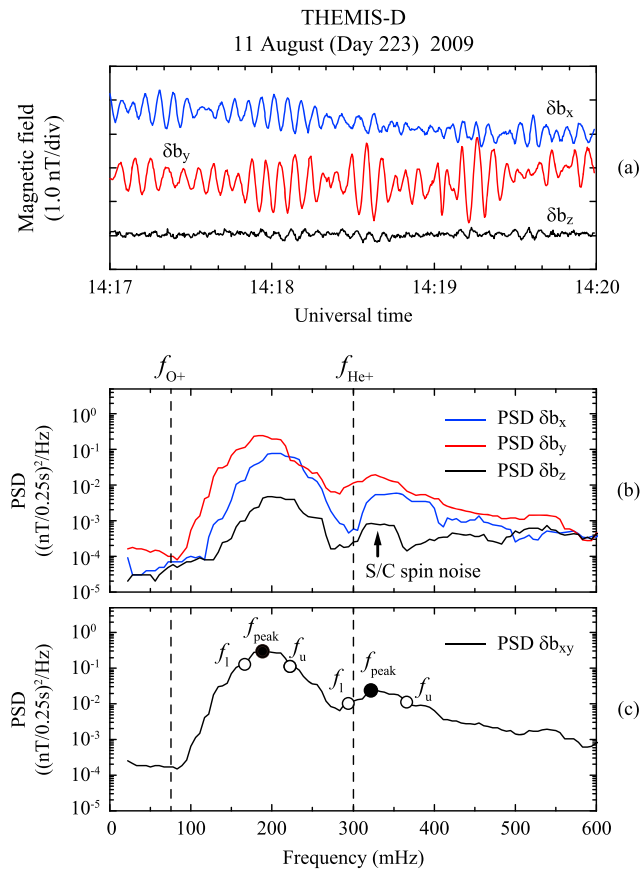


**Figure 3.** (a) The waveforms of the three components ( $\delta b_x$ ,  $\delta b_y$ , and  $\delta b_z$ ) in MFA coordinates for a 3 min period during the intense EMIC wave activity seen in Figure 2. (b) The power spectral densities of transverse components (PSD\_  $\delta b_x$  and PSD\_  $\delta b_y$ ) and compressional component (PSD\_  $\delta b_z$ ). (c) Total transverse power spectral density (PSD\_  $\delta b_{xy}$ ), defined to be PSD\_  $\delta b_x$  + PSD\_  $\delta b_y$ . The solid circles indicate the spectral peak ( $f_{peak}$ ) in PSD\_  $\delta b_{xy}$  in the H-band and He-band, respectively. The spectral width for each peak is marked with open circles.

For the interval of ~13:30–15:15 UT, where  $\Delta B$  gradually increased, the wave activity in the transverse components was strongly enhanced in the He-band. This is consistent with recent studies by *Hyun et al.* [2014] and *Park et al.* [2016]. They reported that the He-band EMIC waves can be excited by small enhancements in  $P_{sw}$  under quiet geomagnetic conditions. A maximum intensity in the He-band occurred at ~14:20 UT. This coincides with the increase in  $N_{sp}$ . The He-band waves suddenly disappeared as the spacecraft exited the plasmasphere. In the low-density region, the wave activity was identified only in the H-band. The He-band EMIC waves were again detected while the spacecraft was in the dense plasmaspheric plasma attached at the magnetopause. The important fact here is that the appearance and disappearance of He-band and H-band EMIC waves are associated with the spatial distribution of cold plasmaspheric plasma. We note that EMIC wave occurrence depending on solar wind dynamic pressure and various geomagnetic conditions identified with *AE* and *SYM-H* has been reported by *Usanova et al.* [2012], who used THEMIS magnetic field data. In this study we mainly focus on the relationship between EMIC wave occurrence and cold plasmaspheric plasma.

Figure 3a shows the waveforms of the three components in MFA coordinates for a 3 min period during the intense EMIC wave activity seen in Figure 2. There are oscillations in all field components, but they are mostly strongly transverse oscillations, as expected from the dynamic spectra of Figure 2, that consist of several wave packet structures. The transverse components,  $\delta b_x$  and  $\delta b_y$ , exhibit EMIC waves superposed on the field variations, which are much slower in period and larger in amplitude than the EMIC waves. To reduce the effect of such slow and large field variations in the frequency domain analysis, differencing is used prior to the Fourier transform for a given time series [e.g., *Anderson et al.*, 1992a; *Park et al.*, 2016].

The power spectral densities of transverse components (PSD\_  $\delta b_x$  and PSD\_  $\delta b_y$ ) and the compressional component (PSD\_  $\delta b_z$ ) are plotted in Figure 3b. A strong peak is seen in PSD\_  $\delta b_y$  at ~190 mHz in the He-band.

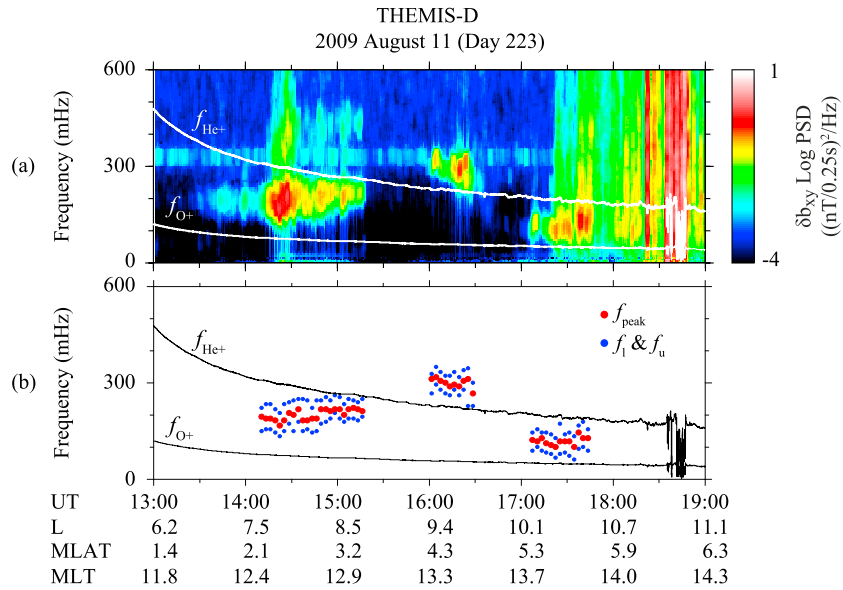


**Figure 4.** (a) The dynamic spectrum of the time-differenced transverse field component ( $\delta b_{xy}$ ) and (b) peak frequency (red dots) of  $\text{PSD}_{\delta b_{xy}}$  with spectral width (blue dots) for EMIC wave events identified using the event selection procedure.

A secondary peak appears in  $\text{PSD}_{\delta b_y}$  at  $\sim 320$  mHz above the local helium gyrofrequency frequency ( $f_{\text{He}^+}$ ) (i.e., in the H-band). The secondary peak is located near the spacecraft spin period ( $\sim 3$  s). By comparing the dynamic spectra of Figure 2 and power spectrum densities in Figure 3b, we confirmed that the spin tone around 330 mHz has a power spectral density of  $\sim 10^{-3}$  in units of  $(\text{nT}/0.25 \text{ s})^2/\text{Hz}$ , which is comparable to the background noise level in the frequency band above  $\sim 300$  mHz. We also confirmed that  $\text{PSD}_{\delta b_y}$  at the secondary peak is larger than the spin tone power by a factor of 15. If our threshold is used to identify EMIC wave activity near 330 mHz, the spin tone does not significantly affect our statistical study.

In order to identify EMIC wave events, we used the following procedure. First, we generated 3 min segments of data covering the outer magnetosphere ( $L > 6$ ) by THEMIS spacecraft and calculated the power spectral density of the three field components. Over this time period, the oscillations should be characterized as predominantly transverse. That is,  $\text{PSD}_{\delta b_x}$  or  $\text{PSD}_{\delta b_y}$  should be larger than  $\text{PSD}_{\delta b_z}$  by a factor of 10 or more. This is a very simple procedure to discriminate against Pc3 pulsations (frequency = 22–100 mHz by definition), generated in the upstream region and propagating into the magnetosphere as fast mode (compressional) waves Hughes [1994]. In the frequency domain analysis, Pc3 pulsations and EMIC waves cannot be distinguished in the outer magnetosphere because the He-band of EMIC waves in that region overlaps with the frequency band of Pc3 pulsations with a short period. Second, we determined the highest spectral peak ( $f_{\text{peak}}$ ) in the total transverse power spectral density ( $\text{PSD}_{\delta b_{xy}}$ ), defined to be  $\text{PSD}_{\delta b_x} + \text{PSD}_{\delta b_y}$ , in the H-band and He-band. Third, the spectral width, marked by  $f_l$  and  $f_u$ , of the  $\text{PSD}_{\delta b_{xy}}$  peak is determined at the level of 50% of the peak power. Both  $f_l$  and  $f_u$  should be in the He-band for He-band EMIC waves and in the H-band for H-band EMIC waves. Finally, we determined the EMIC wave power ( $P_{\text{tr}}$ ) calculated by integrating  $\text{PSD}_{\delta b_{xy}}$  over the frequency band ( $\Delta f$ ) between  $f_l$  and  $f_u$ . The wave power  $P_{\text{tr}}$  should be larger than a power threshold of  $2.0 \times 10^{-4} (\text{nT}/0.25 \text{ s})^2$ .

Figure 3c shows  $\text{PSD}_{\delta b_{xy}}$ ,  $f_{\text{peak}}$  (solid circles), and the width of  $f_{\text{peak}}$  (marked by open circles) for the 3 min interval. The peak powers calculated over  $\Delta f$  in the H-band and He-band are greater than our threshold. However, the H-band EMIC wave event is not selected as a H-band EMIC wave event because  $f_l$  of  $f_{\text{peak}}$  is located in the He-band. It should be noted that only  $\sim 3\%$  of the He-band wave events were identified with the H-band wave events in our statistical study. This result is not surprising. According to Kozyra *et al.* [1984], the H-band wave growth is strongly suppressed by cold heavy ions ( $\text{He}^+$  and  $\text{O}^+$ ) in the plasmaspheric plasmas. As shown in Figures 2 and 3, the wave power in the H-band when both H-band and He-band waves coexist is smaller than the He-band power by a factor of 10. This indicates that the high-density region contains cold heavy ions.

Figure 4 shows the dynamic spectrum of the time-differenced transverse field component ( $\delta b_{xy}$ ) and peak frequency of PSD\_ $\delta b_{xy}$  with  $\Delta f$  for EMIC wave events identified using the above procedure. In the dynamic spectrum, the He-band EMIC wave activities for the interval of  $\sim 13:30$ – $14:10$  UT are visually identified. However, they were not selected as EMIC wave events because their powers calculated in 3 min time windows did not pass our threshold. In our statistical study, EMIC wave activity is required to last more than 10 min (i.e., more than three  $P_{tr}$ ). Once EMIC wave events are selected, their peak frequencies are plotted in the frequency-time format and verified by manually comparing them against the  $\delta b_{xy}$  dynamic spectrum of the format shown in Figure 4. Thus, our event selection procedure is not automatic but instead semiautomatic.

## 4. Statistical Analysis

In this section, we present statistical analyses of EMIC wave events selected using the procedure described in section 3. It should be noted that comprehensive statistical studies of EMIC wave properties using THEMIS spacecraft have been conducted by *Min et al.* [2012] and *Usanova et al.* [2012]. However, *Min et al.* [2012] did not examine whether the spatial distribution of the EMIC wave occurrence depends on geomagnetic activity, and *Usanova et al.* [2012] examined wave occurrence without distinguishing the He-band and H-band EMIC waves. In our statistical study, we investigate the occurrence rate of the He-band and H-band EMIC waves for three different geomagnetic conditions (i.e., all  $Kp$  conditions,  $Kp \geq 2$ , and  $Kp \leq 1$ ). We also examine the relationship between EMIC wave occurrence and cold plasmaspheric plasma distribution because the example shown above indicates that the plasmaspheric plasma is one of the main control parameters for EMIC wave activities.

### 4.1. Spatial Distribution of EMIC Waves

Figures 5a–5c show the distribution of the total observation time of three THEMIS probes in hours for all  $Kp$  conditions, moderate and disturbed conditions ( $Kp \geq 2$ ), and quiet conditions ( $Kp \leq 1$ ), respectively, in  $L$ -MLT coordinates for a 4 year period from 2008 to 2011. Note that the color key scale for all  $Kp$  conditions is different from that for  $Kp \geq 2$  and  $Kp \leq 1$ . The gray circles represent four magnetic  $L$  shells ( $L = 6, 8, 10,$  and  $12$ ). The data coverage is biased to higher values at larger  $L$  because the spacecraft stayed longer near their apogees ( $\sim 10 R_E$ ). The coverage is much higher under quiet geomagnetic conditions ( $Kp \leq 1$ ) than under moderate and disturbed conditions ( $Kp \geq 2$ ). This is due to the fact that a 3 year (2008–2010) period out of a total of 4 year period was in solar minimal activity although solar cycle 24 began in 2008. *Park et al.* [2016] reported that  $\sim 70\%$  of 2007–2008 was under geomagnetic conditions of  $Kp \leq 2$ . Comparing solar cycle 22 and solar cycle 24, *Saikin et al.* [2016] reported that a disproportionate amount of spacecraft dwell time has occurred when geomagnetic activity or solar wind dynamic pressure was considerably quiet or low in solar cycle 24.

Figure 6 shows the spatial distributions of H-band EMIC wave observation time and occurrence rate, calculated by dividing the event observation time by the total observation time for each square bin with  $\Delta x = 1 R_E$  by  $\Delta y = 1 R_E$ , covering all local times from  $L = 6$  to  $L = 12$  for the three different geomagnetic conditions. Regions with an event observation time less than 0.2 h and occurrence rate less than 0.1% appear as white space on the  $L$ -MLT plots. The occurrence rate of H-band EMIC waves for all  $Kp$  increases with  $L$  and is high in the outermost region ( $L = 10$ – $12$ ), suggesting wave generation sources located at large radial distances [e.g., *Anderson et al.*, 1992a; *Usanova et al.*, 2012]. This is quantitatively consistent with previous THEMIS statistics provided by *Min et al.* [2012] except for a region of 0300–0600 MLT for  $L > 10$ . This difference may be due to different thresholds for event selection. In *Min et al.*, the average H-band EMIC wave power in the early morning sector (0600–0900 MLT) for  $L > 10$  is larger than in the early dawn sector (0300–0600 MLT) for  $L > 10$ . Such dawn sector events with weak power may not exceed our threshold. In the occurrence rate distribution of the H-band events for  $Kp \geq 2$  and  $Kp \leq 1$ , we found two important features. One is that the H-band EMIC waves appear more globally in longitude under quiet geomagnetic conditions than under moderate and disturbed conditions. Another notable feature is that the H-band events under quiet geomagnetic conditions ( $Kp \leq 1$ ) mostly contribute to the maximum occurrence rate seen in the early morning sector (0600–0900 MLT) at the outermost region ( $L > 10$ ) for all  $Kp$  conditions. This geomagnetic dependence of the spatial distribution on H-band EMIC wave occurrence has not been reported in *Min et al.* [2012].

The He-band EMIC wave observation time and occurrence rate are plotted in Figure 7, in the same format as Figure 6. Note that the color key scale for H-band events is different from that for He-band events. By comparing the occurrence rates of H-band and He-band waves, we confirm that the overall occurrence rate of the H-band events is higher than the He-band events, consistent with AMPTE/CCE observations [*Keika et al.*, 2013].

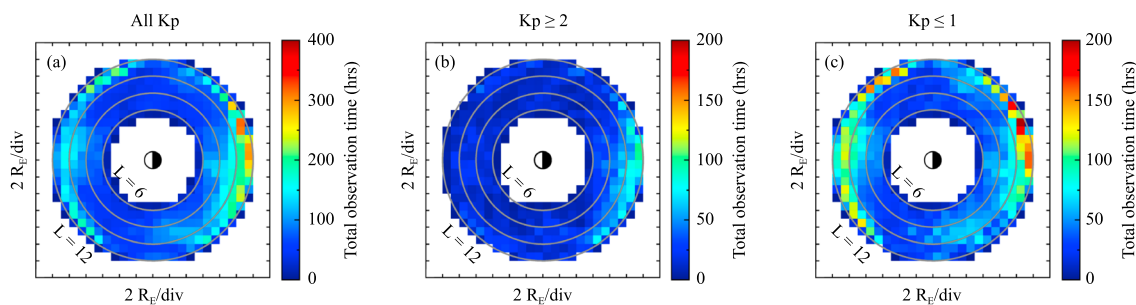


**Figure 5.** The distribution of the total observation time of THEMIS A, D, and E in hours for (a) all  $K_p$  conditions, (b) moderate and disturbed conditions ( $K_p \geq 2$ ), and (c) quiet conditions ( $K_p \leq 1$ ), respectively, in  $L$ -MLT coordinates for a 4 year period from 2008 to 2011.

Unlike the occurrence rate of H-band waves, the occurrence peak of He-band waves for all  $K_p$  is not in the outermost region ( $L > 10$ ) in the morning but in a region of  $L = 8 - 10$  located in the postnoon ( $\sim 1500 - 1600$  MLT) sector. This peak location is similar to the previous THEMIS and AMPTE/CCE observations. In our study, the He-band events are very rare in a region of the midnight-to-early morning sector. Therefore, there is no secondary peak near dawn for  $L > 10$  seen in *Min et al.* [2012]. The discrepancy between our result and that of *Min et al.* should be again reconciled. *Min et al.* reported that the average He-band EMIC wave power in the post-noon sector for  $L > 7$  is much larger than the wave power in a region of 0300–0900 MLT, by a factor of  $\sim 10$ , and that low power He-band EMIC waves near dawn have large normal angles ( $\sim 60^\circ$ ). These waves are characterized as compressional waves in our study. Thus, He-band waves near dawn in *Min et al.* [2012] may not be selected as He-band events in our study. We note that the local time occurrence distribution of He-band waves for all  $K_p$  shown in Figure 7d is very consistent with AMPTE/CCE observations using transverse components to determine EMIC wave activity [*Keika et al.*, 2013] even though the spacecraft apogee is around  $L = 9$  (see Figure 5c in their study).

The He-band waves for  $K_p \geq 2$  are mainly localized between 1200 and 1800 MLT with a peak near postnoon at  $L = 8 - 10$ , and their occurrence rate (note the different color scale) is higher than that for  $K_p \leq 1$ . Under quiet conditions, the wave occurrence distribution extends toward both morningside and nightside. At lower  $L$  values near geosynchronous orbit ( $L \sim 7$ ), the occurrence of quiet-time He-band waves is high near noon. At larger radial distances ( $L \sim 8 - 12$ ), however, higher occurrence appears in the late afternoon. Under quiet conditions, the radial distance of high-occurrence region varies with longitude. Unlike the He-band events for

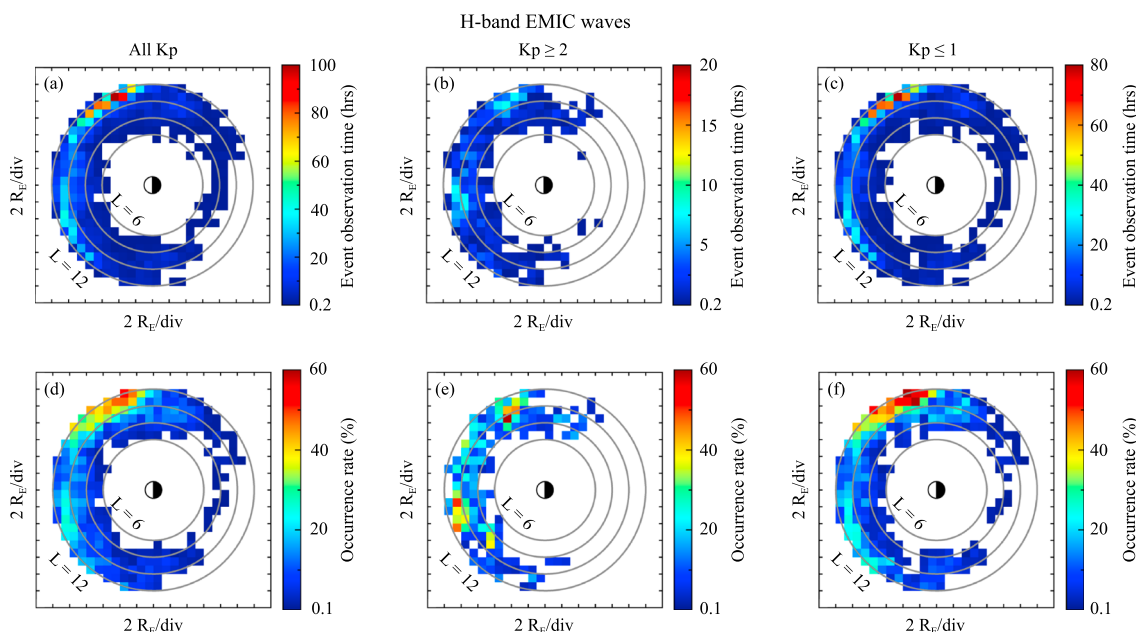


**Figure 6.** Spatial distributions of H-band EMIC wave observation time and occurrence rate (a, d) for all  $K_p$ , (b, e) for  $K_p \geq 2$ , and (c, f) for  $K_p \leq 1$ , respectively.

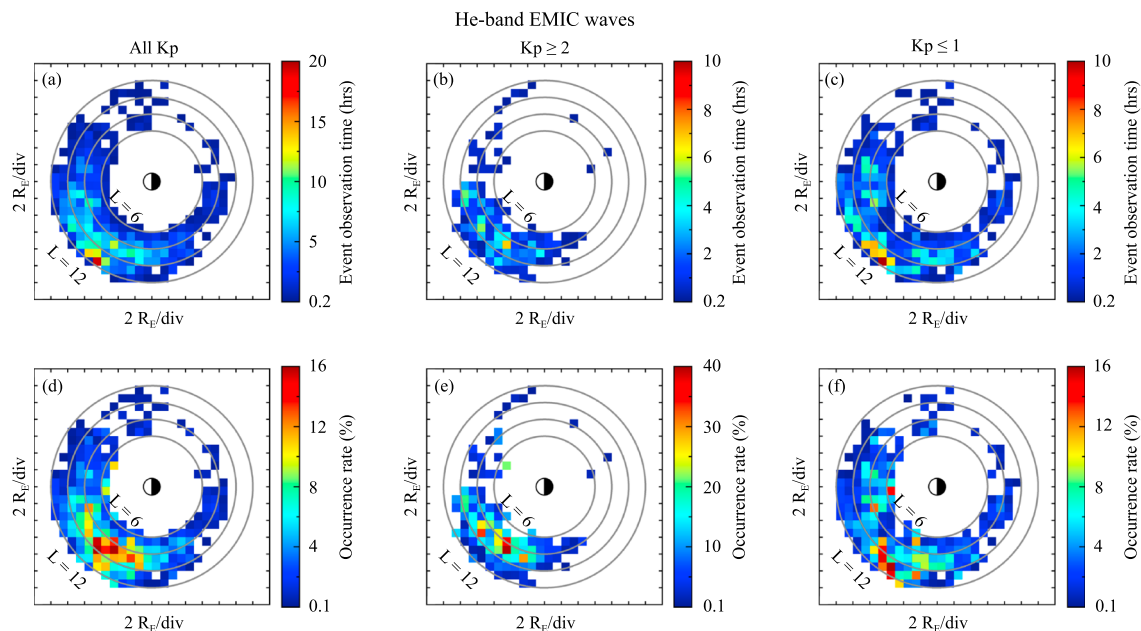


**Figure 7.** The spatial distributions of He-band EMIC wave observation time and occurrence rate in the same format as Figure 6.

$Kp \geq 2$ , the high occurrence rate for  $Kp \leq 1$  extends out to the outermost radial distance region ( $L = 10-12$ ) in the afternoon. These observations indicate that the high-occurrence region of He-band waves depends on geomagnetic activity.

Figures 8a–8c show the  $L$ -MLT maps of the median values of the normalized frequency ( $f_{\text{peak}}/f_{\text{H}^+}$ ) for H-band waves. Information on the geomagnetic activities is also provided for all  $Kp$ ,  $Kp \geq 2$ , and  $Kp \leq 1$ . The notable feature in the map for all  $Kp$  is the strong morning-afternoon asymmetry in the normalized frequency. This morning-afternoon asymmetry does not depend on the geomagnetic activities. The normalized frequency is  $\sim 0.5$  in the morning and  $\sim 0.3$  in the afternoon. These results are consistent with previous THEMIS statistics [Min et al., 2012].

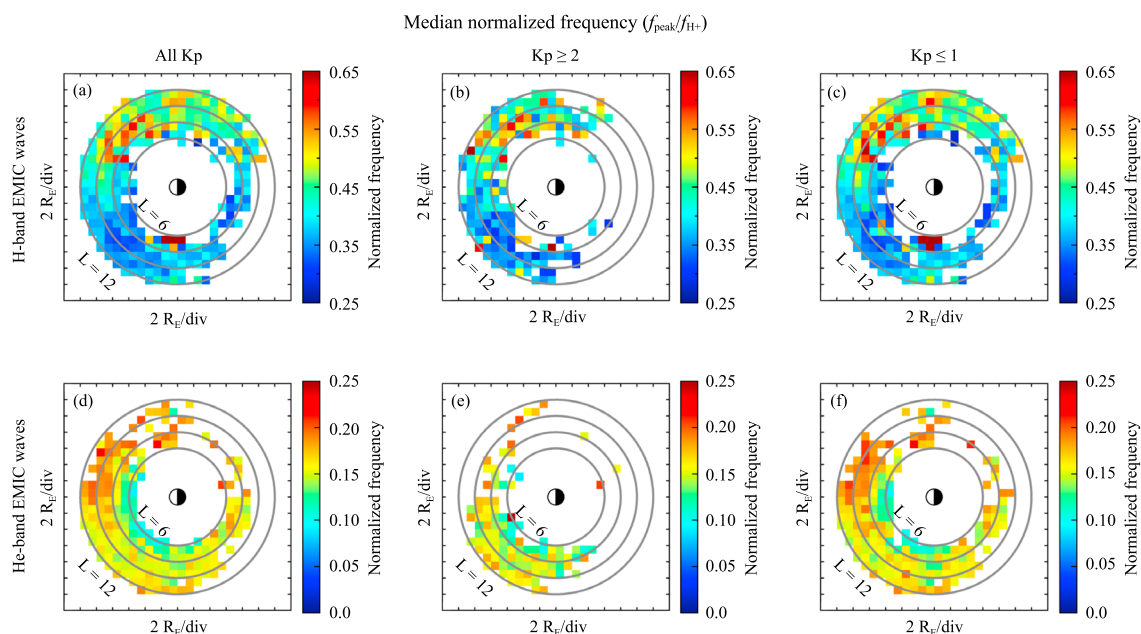


**Figure 8.** (a–c) The  $L$ -MLT maps of the median values of the normalized frequency ( $f_{\text{peak}}/f_{\text{H}^+}$ ) for H-band waves under the three different geomagnetic conditions. (d–f) Same as Figures 8a–8c, except for He-band waves.

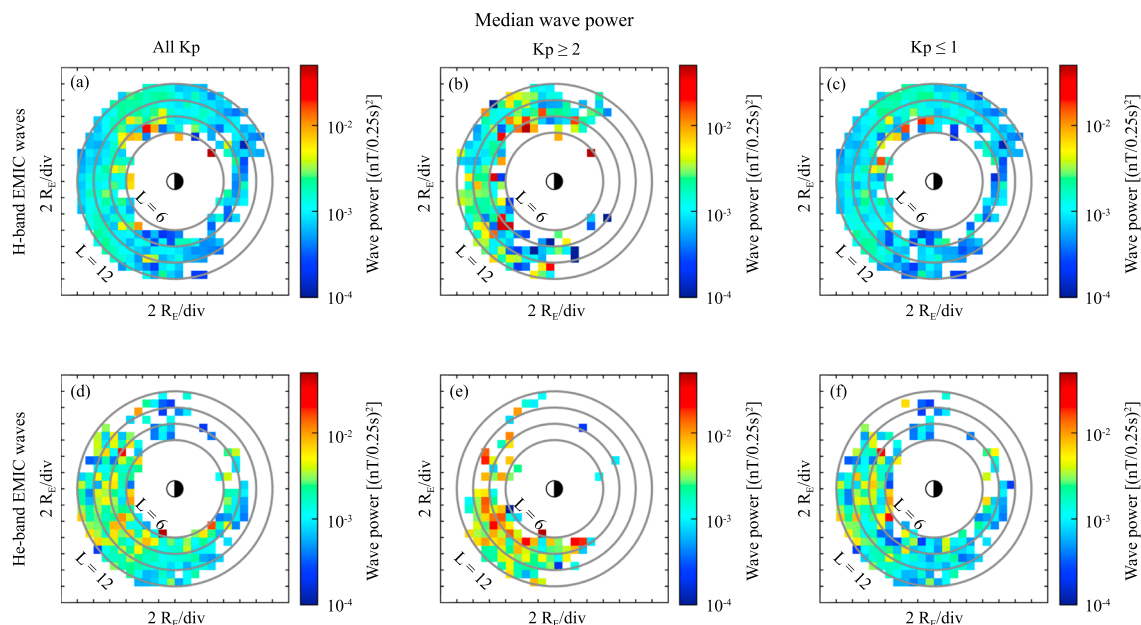


**Figure 9.** The median wave powers of the H-band and He-band events under the three different geomagnetic conditions.

Figures 8d–8f show the normalized frequency for the He-band events. The normalized frequency is clearly higher in the prenoon sector than in the postnoon sector in the outer magnetosphere for  $L > 8$ . This asymmetry is mainly due to the quiet-time He-band waves. Near noon, the normalized frequency of He-band waves decreases monotonically with decreasing radial distance with a minimum of about 0.12 at  $L = 6–7$ . This value is very similar to the medians of the normalized frequency near noon at geosynchronous orbit under quiet geomagnetic conditions [Kim *et al.*, 2016a].

The median wave powers of the H-band and He-band events are plotted in Figure 9. For each geomagnetic activity, it is likely that the location of enhanced wave power is not always consistent with the region where the majority of the EMIC waves occur. As shown in the example (Figures 2 and 3), the EMIC wave power significantly varies from event to event even though the events are observed at near the same location. Thus, median statistics likely do not provide a systematic spatial distribution of wave power. However, there is a clear tendency for the power of EMIC waves to increase under more disturbed geomagnetic conditions. This observation is connected to previous observations reporting that the occurrence rate of EMIC waves increases with geomagnetic activity [e.g., Usanova *et al.*, 2012; Park *et al.*, 2016].

#### 4.2. Cold Plasmaspheric Plasma Distribution and EMIC Waves

Figures 10a–10c show the distribution of the median values of  $N_{sp}$  derived from the spacecraft potential for the total observation time plotted in Figure 5 for the three different  $Kp$  conditions. The median  $N_{sp}$  is clearly lower ( $<1 \text{ cm}^{-3}$ ) at large distances ( $L > 8$ ) in the premidnight-to-noon local time sector ( $\sim 2000–1200 \text{ MLT}$ ) than in the remainder of the local time sector ( $\sim 1–10 \text{ cm}^{-3}$ ) for all  $Kp$  conditions. There is a strong enhancement of  $N_{sp}$  ( $\sim 15–30 \text{ cm}^{-3}$ ) at a radial distance of  $L = 6–8$  in the late afternoon sector ( $\sim 1500–1800 \text{ MLT}$ ). This location is consistent with a region where plumes have been commonly detected [e.g., Darrouzet *et al.*, 2008]. According to Sheeley *et al.* [2001], plasmaspheric density is given by

$$N_{sp} = 10 \times \left(\frac{6.6}{L}\right)^4 \quad (1)$$

where  $L$  is the magnetic shell parameter. Taking this model,  $N_{sp}$  varies from  $15 \text{ cm}^{-3}$  at  $L = 6$  to  $1 \text{ cm}^{-3}$  at  $L = 12$ . Walsh *et al.* [2013] used a threshold for plume identification as twice the value given in equation (1) and found many plumes extending toward the dayside magnetopause. From the results of these studies, we suggest that relative high densities ( $\sim 1–30 \text{ cm}^{-3}$ ) formed over the  $L$  range of 6–12 in the afternoon-to-dusk sector are regions of plasmaspheric plasma extending out to the magnetopause. These regions are called plasmaspheric plumes in this study.

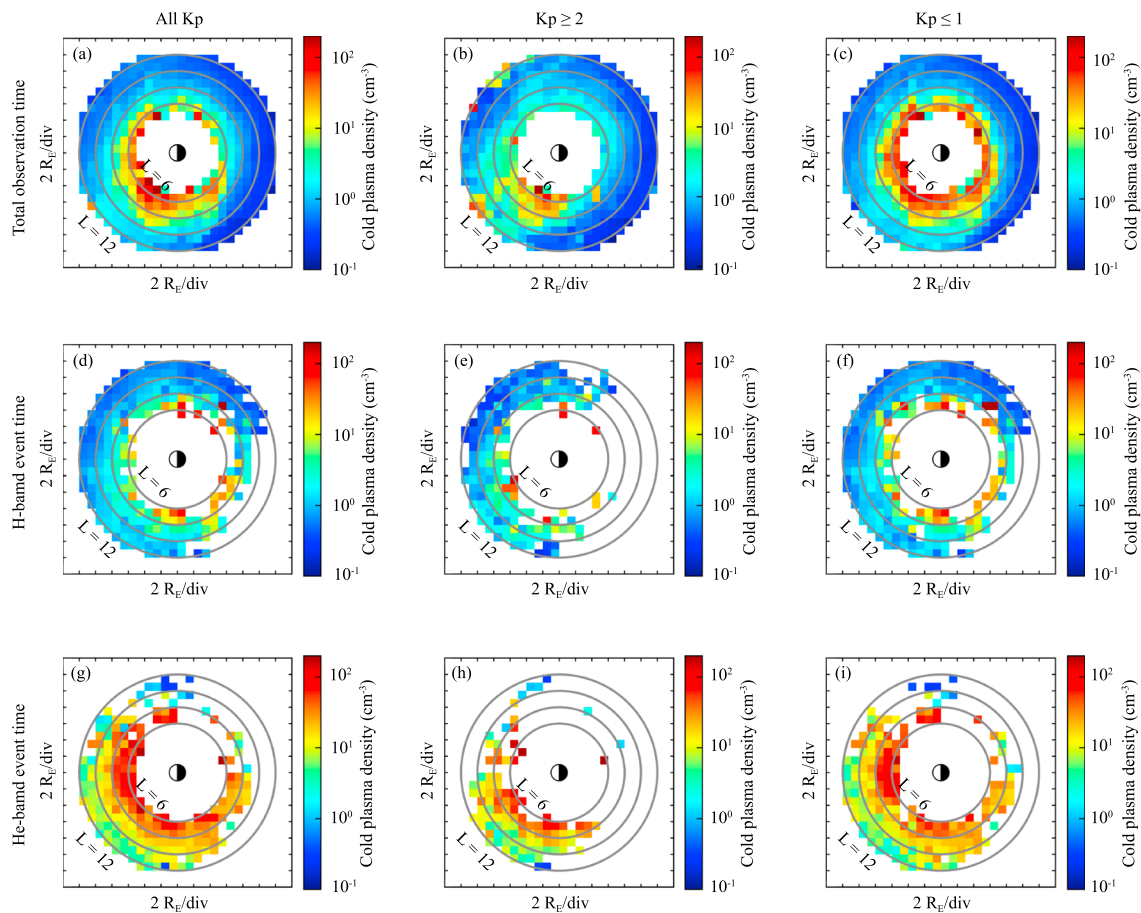


**Figure 10.** (a–c) The distribution of the median values of  $N_{sp}$  derived from the spacecraft potential for the total observation time shown in Figure 5 for the three different  $Kp$  conditions. (d–f) The median values of  $N_{sp}$  during the intervals of the H-band EMIC waves. (g–i) The median values of  $N_{sp}$  during the intervals of the He-band EMIC waves.

Under the moderate and disturbed conditions ( $Kp \geq 2$ ) seen in Figure 10b, the plume structure is more localized along the local time in the afternoon sector from  $L = 6$  to  $L = 12$ . This plume distribution in the  $L$ -MLT map is similar to that reported in previous studies [Darrouzet et al., 2008; Usanova et al., 2013]. High-density regions ( $\sim 20$ – $30 \text{ cm}^{-3}$ ) are strongly localized near the late afternoon (MLT = 1600–1800) for  $L \sim 7$ . This may be associated with the plasmaspheric duskside bulge.

During quiet times ( $Kp \leq 1$ ), the large  $N_{sp}$  enhancement is globally seen at a radial distance between  $L = 6$  and  $L = 8$  along the local time with a dawn-dusk asymmetry. That is, the dusk region has a higher density than the dawn region over the radial distance. The enhanced  $N_{sp}$  sharply decreases around  $L = 8$  near dusk and within  $L = 8$  in other local time sectors. This high-density appearance at  $L = 6$ – $8$  can be interpreted as plasmasphere expansion above  $L = 6$  under quiet conditions [e.g., Moldwin et al., 1994; Kwon et al., 2015]. From a comparison of the radial and longitudinal  $N_{sp}$  distributions for  $Kp \geq 2$  and  $Kp \leq 1$ , we confirm that the duskside plume boundary for  $Kp \geq 2$  expands toward later local times for  $Kp \leq 1$ . The geomagnetic activity dependence of the longitudinal plume distribution is similar to the motion of the plasmaspheric bulge reported by Kwon et al. [2015], who observed that a plasmaspheric bulge shifts toward the postdusk sector from the afternoon sector with decreasing geomagnetic activity.

Figures 10d–10i display the median  $N_{sp}$  derived using  $N_{sp}$  values obtained during the intervals of the H-band and He-band EMIC waves. A major feature evident in the  $N_{sp}$  distributions is that  $N_{sp}$  is much higher for the He-band intervals than for the H-band intervals by a factor of 10 or more, as indicated in the examples in Figure 2. This gives strong support that He-band EMIC wave generation is associated with enhancements in cold plasma density (i.e., in the outer plasmasphere, near the plasmapause, or in plume regions).

Another important feature is that the overall  $N_{sp}$  medians in a region over  $L = 8$  when H-band waves were detected are comparable to the median values of  $N_{sp}$  for the total observation time. There is a clear longitudinal asymmetry in  $N_{sp}$  for H-band events, which is similar to the asymmetric density distribution seen for total observation time (Figure 10a), implying that H-band waves can occur inside or outside the relatively low-density plumes. The H-band  $N_{sp}$  asymmetry for  $Kp \geq 2$  is quantitatively similar to that for  $Kp \leq 1$ . This indicates that the asymmetry is independent of geomagnetic activity.

## 5. Discussion

The most important result of the present study is the fact that a pronounced morning-afternoon asymmetry in the H-band and He-band wave occurrence rates (i.e., frequent occurrence of H-band waves in the morning and He-band waves in the afternoon) is due to the asymmetric distribution of cold plasmaspheric plasma along the local time over large values of  $L$ . We showed that occurrence of the H-band and He-band waves is clearly related to the  $N_{sp}$  values. For each band, we found the morning-afternoon asymmetry of the normalized frequency. This asymmetry is qualitatively similar to the spatial  $N_{sp}$  distribution, implying that the morning-afternoon asymmetry of the frequency is also attributed to the  $N_{sp}$  distribution. In the He-band, the normalized frequency near noon decreases with decreasing radial distance to a minimum at  $L = 6$ , where  $N_{sp}$  is a maximum. From these observations, we can conclude that the cold plasma density plays a significant role in determining the spectral properties of EMIC waves in the outer magnetosphere [Young *et al.*, 1981; Kozyra *et al.*, 1984; Horne and Thorne, 1994].

Our statistical study showed that the occurrence rate of H-band waves increases with radial distance, which is consistent with previous AMPTE/CCE statistics [Anderson *et al.*, 1992a; Keika *et al.*, 2013] and THEMIS statistics [Min *et al.*, 2012; Usanova *et al.*, 2012], which reported that the occurrence of EMIC waves was maximized at higher  $L$  values in the dayside magnetosphere. Under moderate and disturbed geomagnetic conditions ( $Kp \geq 2$ ) in our study, high  $L$  occurrence of the H-band waves mostly appears in the dayside. These observations have been interpreted in terms of EMIC wave growth rate increasing with radial distance [e.g., Anderson *et al.*, 1992a] and magnetospheric compression [e.g., Usanova *et al.*, 2012], leading to an increase in temperature anisotropy of energetic ions.

In the outermost region ( $L > 10$ ), the H-band occurrence rate peaks in the early morning under quiet geomagnetic conditions ( $Kp \leq 1$ ). Such morningside H-band events were less frequently observed for  $Kp \geq 2$ . Both the local time dependence and geomagnetic activity dependence of the H-band occurrence distribution for larger  $L$  ( $> 10$ ) were not reported in previous statistical studies. A possible explanation for quiet-time morningside H-band waves is the outer related to lower part of energetic plasma sheet ions ( $< 10$  keV), which was proposed by Keika *et al.* [2013]. Since such lower energy ions are not sufficiently energetic for their gradient and curvature drifts, the particle motions are dominated by the  $\mathbf{E} \times \mathbf{B}$  drift. The lower energy ions from the magnetotail are convected toward dayside, passing through both dawn and dusk.  $N_{sp}$  is higher in the duskside than in the dawnside, as shown in Figure 10c. If the cold plasmaspheric plasma contains heavy ions (primarily  $O^+$  and  $He^+$ ), the H-band growth rate in the duskside is strongly suppressed [Kozyra *et al.*, 1984]. Recently, Hyun *et al.* [2014] and Park *et al.* [2016] reported that EMIC waves can be readily generated with small  $P_{sw}$  enhancements under quiet geomagnetic conditions. Since magnetospheric compression has a large effect on the region close to the magnetopause, the occurrence rate of H-band waves is higher in the morning than in the afternoon in the outermost region under quiet conditions, as seen in Figure 6f. The H-band occurrence distribution is not continuous along the magnetic local time from dawn to dusk for  $L > 10$ . That is, there is a longitudinal separation near noon. This may be due to the fact that the plasma sheet ions are not on closed drift paths.

The He-band waves for all  $Kp$ , shown in Figure 7d, mostly occur in the postnoon sector with a peak around 1500–1600 MLT. Unlike the H-band waves, the He-band peak occurrence along the radial direction is not at the outermost location ( $L = 10–12$ ), but instead at the radial distances of  $L = 8–10$ , indicating that the preferred region for He-band EMIC wave generation is different from that for H-band generation. The spatial distribution of  $N_{sp}$  shown in Figure 10 contains important clues about the occurrence of He-band waves. Comparing the peak occurrence region of the He-band events and the radial distribution of  $N_{sp}$  for the three levels of  $Kp$ , we found that a preferred He-band wave occurrence appears at a steep  $N_{sp}$  gradient region, which is considered to be the plasmopause or plume boundary, near  $L = 7–10$  along the local time. These results support previous theoretical studies reporting that enhanced wave growth occurs within regions of spatial overlap

of anisotropic ring current ions and high-density cold plasma regions just inside the plasmopause or plumes [e.g., Cornwall *et al.*, 1970; Kozyra *et al.*, 1984; Thorne *et al.*, 2006; Chen *et al.*, 2009].

Under quiet geomagnetic conditions, the He-band occurrence rate is higher around noon at lower  $L$  values of  $\sim 6$ –8. In that region,  $N_{sp}$  is at its highest ( $\sim 100 \text{ cm}^{-3}$ ), indicating that He-band EMIC waves occur just inside or near the plasmopause. The longitudinal peak location at this radial distance is consistent with a recent study reported by Park *et al.* [2016], who examined the occurrence probability of quiet-time He-band EMIC waves using geosynchronous magnetometer data. They observed that quiet-time geosynchronous He-band waves mostly occur in the region from morning to afternoon, with a peak around noon, and suggested that the major driver of the He-band waves is solar wind pressure variations, even for small enhancements. A higher occurrence near noon at  $L = 6$ –8 indicates that the plasmasphere expanded frequently, approaching the geosynchronous region, under quiet geomagnetic conditions [Kwon *et al.*, 2015]. In the late afternoon sector, the higher-occurrence region is distributed over large radial distances between  $L = 8$  and  $L = 12$ . This may be due to the fact that density gradients occur more broadly with radial distance. Kwon *et al.* [2015] observed that the plasmopause location under quiet conditions ( $Kp \leq 1$ ) is highly scattered between  $L = 4$  and  $L = 10$  in the postnoon-to-midnight sector. The He-band occurrence distribution extending to midnight under quiet conditions can be explained by the longitudinal distribution of quiet-time plasmopause locations reported by Kwon *et al.* (see Figure 4 in their study).

There have been statistical studies on the relationship between the occurrence of EMIC waves and plasmaspheric plumes [Posch *et al.*, 2010; Usanova *et al.*, 2013]. They reported that the occurrence of EMIC waves has a weak correlation with the occurrence of plasmaspheric plumes. In their studies, however, they examined EMIC waves without distinguishing the H-band and He-band. Our statistical results clearly show that  $N_{sp}$  was relatively low when H-band EMIC waves were detected and that H-band waves occur globally both inside and outside low-density plumes. Since the occurrence rate of H-band waves is higher than that of He-band waves in the outer magnetosphere above  $L = 6$ , the correspondence between the occurrence of He-band waves and plumes may be smeared in the previous studies.

## 6. Conclusion

We have examined the properties of EMIC waves in the outer magnetosphere using THEMIS data over a 4 year period from 2008 to 2011. We have shown that the spatial distribution of H-band and He-band wave occurrence rates depends on geomagnetic activity. By comparing the cold plasma distribution with the EMIC wave occurrence and normalized frequency, we confirmed that the morning-afternoon asymmetries of H-band and He-band EMIC wave occurrence rate and normalized frequency for each band are associated with the cold plasma density distribution. Our major finding is that the cold plasma density is much higher for the He-band wave intervals than for the H-band wave intervals by a factor of 10 or more. These observations indicate that the cold plasma density plays a significant role in determining the spectral properties of EMIC waves in the outer magnetosphere.

### Acknowledgments

The THEMIS data used in this study were obtained from the THEMIS website (<http://themis.ssl.berkeley.edu>). The geomagnetic  $Kp$  index was provided by the World Data Center C2 (WDC-C2) for Geomagnetism, Kyoto University (<http://wdc.kugi.kyoto-u.ac.jp/index.html>). The solar wind and interplanetary magnetic field (IMF) data were obtained from OMNI Website (<http://omniweb.gsfc.nasa.gov>). This work was supported by BK21+ through the National Research Foundation (NRF) funded by the Ministry of Education of Korea and also supported by project PE16090 of the Korea Polar Research Institute. The work of K.-H. Kim was supported by the Basic Science Research Program through NRF funded by NRF-2016R1A2B4011553.

### References

- Allen, R. C., J.-C. Zhang, L. M. Kistler, H. E. Spence, R.-L. Lin, B. Klecker, M. W. Dunlop, M. Andre, and V. K. Jordanova (2015), A statistical study of EMIC waves observed by Cluster: 1. Wave properties, *J. Geophys. Res. Space Physics*, *120*, 5574–5592, doi:10.1002/2015JA021333.
- Allen, R. C., J.-C. Zhang, L. M. Kistler, H. E. Spence, R.-L. Lin, B. Klecker, M. W. Dunlop, M. Andre, and V. K. Jordanova (2016), A statistical study of EMIC waves observed by Cluster: 2. Associated plasma conditions, *J. Geophys. Res. Space Physics*, *121*, 6458–6479, doi:10.1002/2016JA022541.
- Anderson, B. J., R. E. Erlandson, and L. J. Zanetti (1992a), A statistical study of Pc 1–2 magnetic pulsations in the equatorial magnetosphere: 1. Equatorial occurrence distributions, *J. Geophys. Res.*, *97*(A3), 3075–3088, doi:10.1029/91JA02706.
- Anderson, B. J., R. E. Erlandson, and L. J. Zanetti (1992b), A statistical study of Pc 1–2 magnetic pulsations in the equatorial magnetosphere: 2. Wave properties, *J. Geophys. Res.*, *97*(A3), 3089–3101, doi:10.1029/91JA02697.
- Anderson, B. J., and D. C. Hamilton (1993), Electromagnetic ion cyclotron waves stimulated by modest magnetospheric compressions, *J. Geophys. Res.*, *98*(A7), 11,369–11,382, doi:10.1029/93JA00605.
- Arnoldy, R. L., et al. (2005), Pc 1 waves and associated unstable distributions of magnetospheric protons observed during a solar wind pressure pulse, *J. Geophys. Res.*, *110*, A07229, doi:10.1029/2005JA011041.
- Auster, H. U., et al. (2008), The THEMIS fluxgate magnetometer, *Space Sci. Rev.*, *141*(1–4), 235–264, doi:10.1007/s11214-008-9365-9.
- Bonnell, J. W., F. S. Mozer, G. T. Delory, A. J. Hull, R. E. Ergun, C. M. Cully, V. Angelopoulos, and P. R. Harvey (2008), The Electric Field Instrument (EFI) for THEMIS, *Space Sci. Rev.*, *141*, 303–341, doi:10.1007/s11214-008-9469-2.
- Bossen, M., R. L. McPherron, and C. T. Russell (1976), Simultaneous Pc 1 observations by the synchronous satellite ATS-1 and ground stations: Implications concerning IPDP generation mechanism, *J. Atmos. Sol. Terr. Phys.*, *38*, 1157–1167.
- Carpenter, D. L., and R. R. Anderson (1992), An ISEE/whistler model of equatorial electron density in the magnetosphere, *J. Geophys. Res.*, *97*, 1097–1108.

- Chen, L., R. M. Thorne, and R. B. Horne (2009), Simulation of EMIC wave excitation in a model magnetosphere including structured high-density plumes, *J. Geophys. Res.*, *114*, A07221, doi:10.1029/2009JA014204.
- Clausen, L. B. N., J. B. H. Baker, J. M. Ruohoniemi, and H. J. Singer (2011), EMIC waves observed at geosynchronous orbit during solar minimum: Statistics and excitation, *J. Geophys. Res.*, *116*, A10205, doi:10.1029/2011JA016823.
- Cornwall, J. M. (1965), Cyclotron instabilities and electromagnetic emission in the ultra low frequency and very low frequency ranges, *J. Geophys. Res.*, *70*(1), 61–69, doi:10.1029/JZ070i001p00061.
- Cornwall, J. M., F. V. Coroniti, and R. M. Thorne (1970), Turbulent loss of ring current protons, *J. Geophys. Res.*, *75*(25), 4699–4709, doi:10.1029/JA075i025p04699.
- Darrrouzet, F., J. De Keyser, P. M. E. Decreau, F. El Lemdani-Mazouz, and X. Vallieres (2008), Statistical analysis of plasmaspheric plumes with Cluster/WHISPER observations, *Ann. Geophys.*, *26*(8), 2403–2417.
- Engebretson, M. J., W. K. Peterson, J. L. Posch, M. R. Klatt, B. J. Anderson, C. T. Russell, H. J. Singer, R. L. Arnoldy, and H. Fukunishi (2002), Observations of two types of Pc 1–2 pulsations in the outer dayside magnetosphere, *J. Geophys. Res.*, *107*(A12), 1451, doi:10.1029/2001JA000198.
- Fraser, B. J., W. J. Kemp, and D. J. Webster (1989), Ground-satellite study of a Pc 1 ion cyclotron wave event, *J. Geophys. Res.*, *94*, 11,855–11,863.
- Fraser, B. J., and T. S. Nguyen (2001), Is the plasmapause a preferred source region of electromagnetic ion cyclotron waves in the magnetosphere?, *J. Atmos. Sol. Terr. Phys.*, *63*, 1225–1247.
- Halford, A. J., B. J. Fraser, S. K. Morley, S. R. Elkington, and A. A. Chan (2016), Dependence of EMIC wave parameters during quiet, geomagnetic storm, and geomagnetic storm phase times, *J. Geophys. Res. Space Physics*, *121*, 6277–6291, doi:10.1002/2016JA022694.
- Horne, R. B., and R. M. Thorne (1994), Convective instabilities of electromagnetic ion cyclotron waves in the outer magnetosphere, *J. Geophys. Res.*, *99*(A9), 17,259–17,273.
- Hughes, W. J. (1994), Magnetospheric ULF waves: A tutorial with a historical perspective, in *Solar Wind Sources of Magnetospheric Ultra-Low-Frequency Waves*, *Geophys. Monogr. Ser.*, vol. 81, edited by M. J. Engebretson, K. Takahashi, and M. Scholer, pp. 1–11, AGU, Washington, D. C.
- Hyun, K., K.-H. Kim, E. Lee, H.-J. Kwon, D.-H. Lee, and H. Jin (2014), Loss of geosynchronous relativistic electrons by EMIC wave scattering under quiet geomagnetic conditions, *J. Geophys. Res. Space Physics*, *119*, 8357–8371, doi:10.1002/2014JA020234.
- Kasahara, Y., A. Sawada, M. Yamamoto, I. Kimura, S. Kokubun, and K. Hayashi (1992), Ion cyclotron emissions observed by the satellite Akebono in the vicinity of the magnetic equator, *Radio Sci.*, *27*(2), 347–362, doi:10.1029/91RS01872.
- Keika, K., K. Takahashi, A. Y. Ukhorskiy, and Y. Miyoshi (2013), Global characteristics of electromagnetic ion cyclotron waves: Occurrence rate and its storm dependence, *J. Geophys. Res. Space Physics*, *118*, 4135–4150, doi:10.1002/jgra.50385.
- Kennel, C. F., and H. E. Petschek (1966), Limit on stably trapped particle fluxes, *J. Geophys. Res.*, *71*(1), 1–28.
- Kim, K.-H., J.-S. Park, Y. Omura, K. Shiokawa, D.-H. Lee, G.-J. Kim, H. Jin, E. Lee, and H.-J. Kwon (2016a), Spectral characteristics of steady quiet-time EMIC waves observed at geosynchronous orbit, *J. Geophys. Res. Space Physics*, *121*, doi:10.1002/2016JA022957.
- Kim, K.-H., K. Shiokawa, I. R. Mann, J.-S. Park, H.-J. Kwon, K. Hyun, H. Jin, and M. Connors (2016b), Longitudinal frequency variation of long-lasting EMIC Pc1–Pc2 waves localized in the inner magnetosphere, *Geophys. Res. Lett.*, *43*, 1039–1046, doi:10.1002/2015GL067536.
- Kozyra, J. U., T. E. Cravens, F. Nagy, E. G. Fonthelm, and R. S. B. Ong (1984), Effects of energetic heavy ions on electromagnetic ion cyclotron wave generation in the plasmapause region, *J. Geophys. Res.*, *89*(A4), 2217–2233, doi:10.1029/JA089iA04p02217.
- Kwon, H.-J., K.-H. Kim, G. Jee, J.-S. Park, H. Jin, and Y. Nishimura (2015), Plasmapause location under quiet geomagnetic conditions ( $Kp \leq 1$ ): THEMIS observations, *Geophys. Res. Lett.*, *42*, 7303–7310, doi:10.1002/2015GL066090.
- Li, W., R. M. Thorne, J. Bortnik, Y. Nishimura, V. Angelopoulos, L. Chen, J. P. McFadden, and J. W. Bonnell (2010), Global distributions of suprathermal electrons observed on THEMIS and potential mechanisms for access into the plasmasphere, *J. Geophys. Res.*, *115*, A00J10, doi:10.1029/2010JA015687.
- Lin, R.-L. et al. (2014), Testing linear theory of EMIC waves in the inner magnetosphere: Cluster observations, *J. Geophys. Res. Space Physics*, *119*, 1004–1027, doi:10.1002/2013JA019541.
- McCollough, J. P., S. R. Elkington, and D. N. Baker (2012), The role of Shabansky orbits in compression-related electromagnetic ion cyclotron wave growth, *J. Geophys. Res.*, *117*, A01208, doi:10.1029/2011JA016948.
- McFadden, J. P., C. W. Carlson, D. Larson, M. Ludlam, R. Abiad, B. Elliott, P. Turin, M. Marckwordt, and V. Angelopoulos (2008), The THEMIS ESA plasma instrument and in-flight calibration, *Space Sci. Rev.*, *141*, 277–302, doi:10.1007/s11214-008-9440-2.
- Meredith, N. P., R. M. Thorne, R. B. Horne, D. Summers, B. J. Fraser, and R. R. Anderson (2003), Statistical analysis of relativistic electron energies for cyclotron resonance with EMIC waves observed on CRRES, *J. Geophys. Res.*, *108*(A6), 1250, doi:10.1029/2002JA009700.
- Min, K., J. Lee, K. Keika, and W. Li (2012), Global distribution of EMIC waves derived from THEMIS observations, *J. Geophys. Res.*, *117*, A05219, doi:10.1029/2012JA017515.
- Moldwin, M. B., M. F. Thomsen, S. J. Bame, D. J. McComas, and K. R. Moore (1994), An examination of the structure and dynamics of the outer plasmasphere using multiple geosynchronous satellites, *J. Geophys. Res.*, *99*, 11,475–11,481, doi:10.1029/93JA03526.
- Moldwin, M. B., L. Downward, H. K. Rassoul, R. Amin, and R. R. Anderson (2002), A new model of the location of the plasmapause: CRRES results, *J. Geophys. Res.*, *107*(A11), 1339, doi:10.1029/2001JA009211.
- Nishimura, Y., et al. (2013), Structures of dayside whistler-mode waves deduced from conjugate diffuse aurora, *J. Geophys. Res. Space Physics*, *118*, 664–673, doi:10.1029/2012JA018242.
- Olson, J. V., and L. C. Lee (1983), Pc1 wave generation by sudden impulses, *Planet. Space Sci.*, *31*(3), 295–302, doi:10.1016/0032-0633(83)90079-X.
- Park, J.-S., K.-H. Kim, K. Shiokawa, D.-H. Lee, E. Lee, H.-J. Kwon, H. Jin, and G. Jee (2016), EMIC waves observed at geosynchronous orbit under quiet geomagnetic conditions ( $Kp \leq 1$ ), *J. Geophys. Res. Space Physics*, *121*, 1377–1390, doi:10.1002/2015JA021968.
- Posch, J. L., M. J. Engebretson, M. T. Murphy, M. H. Denton, M. R. Lessard, and R. B. Horne (2010), Probing the relationship between electromagnetic ion cyclotron waves and plasmaspheric plumes near geosynchronous orbit, *J. Geophys. Res.*, *115*, A11205, doi:10.1029/2010JA015446.
- Saikin, A. A., J.-C. Zhang, R. C. Allen, C. W. Smith, L. M. Kistler, H. E. Spence, R. B. Torbert, C. A. Kletzing, and V. K. Jordanova (2015), The occurrence and wave properties of  $H^+$ ,  $He^+$ , and  $O^+$ -band EMIC waves observed by the Van Allen Probes, *J. Geophys. Res. Space Physics*, *120*, 7477–7492, doi:10.1002/2015JA021358.
- Saikin, A. A., J.-C. Zhang, C. W. Smith, H. E. Spence, R. B. Torbert, and C. A. Kletzing (2016), The dependence on geomagnetic conditions and solar wind dynamic pressure of the spatial distributions of EMIC waves observed by the Van Allen Probes, *J. Geophys. Res. Space Physics*, *121*, 4362–4377, doi:10.1002/2016JA022523.

- Sakaguchi, K., K. Shiokawa, Y. Miyoshi, Y. Otsuka, T. Ogawa, K. Asamura, and M. Connors (2008), Simultaneous appearance of isolated auroral arcs and Pc 1 geomagnetic pulsations at subauroral latitudes, *J. Geophys. Res.*, *113*, A05201, doi:10.1029/2007JA012888.
- Sheeley, B. W., M. B. Moldwin, H. K. Rassoul, and R. R. Anderson (2001), An empirical plasmasphere and trough density model: CRRES observations, *J. Geophys. Res.*, *106*(A11), 25,631–25,641, doi:10.1029/2000JA000286.
- Sibeck, D. G., and V. Angelopoulos (2008), THEMIS science objectives and mission phases, *Space Sci. Rev.*, *141*, 35–59, doi:10.1007/s11214-008-9393-5.
- Thorne, R. M., R. B. Horne, V. K. Jordanova, J. Bortnik, and S. Glauert (2006), Interaction of EMIC waves with thermal plasma and radiation belt particles, in *Magnetospheric ULF Waves: Synthesis and New Directions*, *Geophys. Monogr. Ser.*, vol. 169, edited by K. Takahashi et al., pp. 213–224, AGU, Washington, D. C.
- Tsyganenko, N. A., and M. I. Sitnov (2005), Modeling the dynamics of the inner magnetosphere during strong geomagnetic storms, *J. Geophys. Res.*, *110*(A03208), doi:10.1029/2004JA010798.
- Usanova, M. E., I. R. Mann, I. J. Rae, Z. C. Kale, V. Angelopoulos, J. W. Bonnell, K. H. Glassmeier, H. U. Auster, and H. J. Singer (2008), Multipoint observations of magnetospheric compression-related EMIC Pc1 waves by THEMIS and CARISMA, *Geophys. Res. Lett.*, *35*, L17S25, doi:10.1029/2008GL034458.
- Usanova, M. E., I. R. Mann, J. Bortnik, L. Shao, and V. Angelopoulos (2012), THEMIS observations of electromagnetic ion cyclotron wave occurrence: Dependence on AE, SYMH, and solar wind dynamic pressure, *J. Geophys. Res.*, *117*, A10218, doi:10.1029/2012JA018049.
- Usanova, M. E., F. Darrouzet, I. R. Mann, and J. Bortnik (2013), Statistical analysis of EMIC waves in plasmaspheric plumes from Cluster observations, *J. Geophys. Res. Space Physics*, *118*, 4946–4951, doi:10.1002/jgra.50464.
- Walsh, B. M., D. G. Sibeck, Y. Nishimura, and V. Angelopoulos (2013), Statistical analysis of the plasmaspheric plume at the magnetopause, *J. Geophys. Res. Space Physics*, *118*, 4844–4851, doi:10.1002/jgra.50458.
- Wang, D., et al. (2015), Statistical characteristics of EMIC waves: Van Allen Probe observations, *J. Geophys. Res. Space Physics*, *120*, 4400–4408, doi:10.1002/2015JA021089.
- Yahnina, T. A., A. G. Yahnin, J. Kangas, and J. Manninen (2000), Proton precipitation related to Pc1 pulsations, *Geophys. Res. Lett.*, *27*(21), 3575–3578.
- Young, D. T., S. Perraut, A. Roux, C. de Villedary, R. Gendrin, A. Korth, G. Kremser, and D. Jones (1981), Wave-particle interactions near  $\Omega_{\text{He}^+}$  observed on GEOS 1 and 2: 1. Propagation of ion cyclotron waves in He<sup>+</sup>-rich plasma, *J. Geophys. Res.*, *86*(A8), 6755–6772, doi:10.1029/JA086iA08p06755.